Non-contact Non-invasive Heart and Respiration Rates Monitoring with MIMO Radar Sensing

Qiwei Liu, Hanqing Guo, Aron Kageza,
Junhong Xu, Saeed AlQarni, Shaoen Wu
Department of Computer Science
Ball State University
Muncie, IN USA
{qliu4, hguo, agkageza, jxu7, saalqarni, swu}@bsu.edu

Honggang Wang
Dept. of Electrical and Computer Engineering
University of Massachusetts Dartmouth
Dartmouth, MA USA
hwang1@umassd.edu

Abstract—Smart health calls for novel approaches to detect vital signs in non-contact, non-invasive and non-intrusive matters. In this work, we design a solution that monitors the rates of heartbeats and respiration simultaneously by using a Frequency Modulated Continuous Wave (FMCW) radar with multiple antennas. This solution measures the reflections from heartbeats and respiration at a high frequency of $4\ KHz$ to capture fine dynamics of motions with big data. It employs multiple antennas and superposition to reduce the interference noises from unwanted motions in the background and any detection defects. The heart and respiration rates are detected in the frequency domains after a chain of preprocessing techniques on the sensed big data. With extensive experiments in a lab office, this system demonstrates high accuracies in various cases: 98% in the still case, 95% with finger motions and 96% with body motions. The tests also confirm that multiple antennas and signal superposition improve the detection accuracy and reliability.

Index Terms—smart health; wireless sensing; signal processing; big data

I. INTRODUCTION

The development of internet of things (IoT) has already changed people's life. For example, smart security cameras can warn users of unfamiliar visitors; smart thermostats automatically adjust the settings based on temperature, occupancy and user preferences, which doesn't require user's manual effort. Along with the IoT advances is smart health that plays an increasingly significant role in daily life. If a smart environment can monitor human vital signs, potential health problems can be identified in advance. People can be woken up when life threats happen during the sleep, e.g., the cardiac arrhythmia, to save their lives.

Current health monitoring devices, such as finger pulse oximeters and smartwatches, require to install on human bodies, which results in cumbersomeness to wear and uncomfortable or inconvenient experiences. Most of the devices are to obtain a specific vital sign such as heart or respiration rates, but not multiple signs at one time. Many research efforts have investigated non-contact approaches to health monitoring by using wireless sensing such as Doppler radars [1], Ultra-band radars [2], which correlates the distance variations to the motions of hearts. However, those methods are too vulnerable and sensitive to any extraneous motions, e.g., arm or finger motions, so that the accuracy is not consistent.

In this project, we propose a non-contact health monitoring system that can simultaneously detect both heart and respiration rates by using FMCW (Frequency Modulated Continuous Wave) sensing [3] at a very low cost of energy. The system transmits a FMCW wireless signal towards a human subject and receives the reflections. Because the amplitudes of the wireless signals reflected by the body vary in patterns from the periodic chest and heart movements, the heart rate and respiration rate can be obtained from the continuously sampled amplitude variations after cleaning any extraneous motions. Even though the amplitudes are influenced by the compound movements of the heart, chest, and even environmental noises, heart and respiration rates can be still extracted and separated because the patterns in amplitude variations, which can be transformed into frequency domains, are robust to the changes of amplitude value. The detection happens in the frequency domain of the amplitude measurements. After reducing noises and excluding unwanted frequencies from the target frequency range, the frequencies of the peak magnitude in the FFT (Fast Fourier Transform) spectrum that shows the periodicity of the time-series measurements correspond to the heart rate or the respiration rate. Furthermore, to improve accuracy, our system for the first time employs multiple antenna pairs. Those antenna pairs work simultaneously to capture the reflections in different layouts and different ranges.

In short, this work has the following novelties.

- Our solution simultaneously detects the heart and respiration rates from the same amplitude measurements of wireless signals.
- It is the first work that employs MIMO radar sensing with multiple pairs of antennas to improve the detection accuracy and minimize the environmental exceptions and interferences

In the rest, Section II briefs the literature and related work of heart and respiration rate detection. Next, Section III presents the detailed methodology, including how to make use of multiple antennas pairs, eliminate noises and perform the detection. Then, Section IV evaluates the performance on the noise elimination and detection accuracy, which is followed by the conclusion of this work in Section V.

II. RELATED WORK

The progress of Internet of Things (IoT) has made it possible to build an IoT health care system, equipped with sensor networks, to change the way how physicians delivery care and benefit patients. Various non-contact non-invasive methods of monitoring vital signs have been investigated in the past few years, which fall into three areas: radio-based systems, vision-based analysis, and optical-based techniques.

The radio-based systems include the uses of Doppler radars [1], [4], [5], WiFi [6]–[8], and Ultra-band radars [2], [9]. The radio-based systems estimate minute displacements of hearts, requiring a high spatial resolution, resulting in expensive, heavy apparatus and extra energy cost [10]. Due to the lack of the capability to focus on particular spatial range, any irrelevant motions will overwhelm the target signals.

The vision-based analyses amplify patterns extracted from time-lapse images using cameras to extract vital signs [11]–[13]. However, it doesn't work in dark environments. Cameras cannot see through people covered with a quilt during sleeping either. Another issue with this type of approaches is the concern of privacy with all personal activities are monitored.

The optic-based techniques track speckle patterns illuminated by a laser beam on the human skin [14]–[16]. It encounters the same issue as the vision-based method when applies to sleeping scenarios. Moreover, the laser light can be easily blocked to work effectively.

FMCW radars have been widely and long used for military purposes. One strength of FMCW radars is its ability to separate reflections from different objects and allows excluding extraneous motions out of target spatial ranges, and extracting vital signs from amplitude changes caused by compound movements of the heart and chest simultaneously. It does not need an extremely high spatial resolution to differentiate two type of movements.

III. SYSTEM DESIGN

In our proposed solution, a wireless signal is periodically emitted and its reflected signals are captured by multiple antennas and are reported in amplitudes. The amplitudes are first preprocessed to retain only the reflections from the motions of hearts and breaths by removing static background reflections. Then a bandpass filter is applied to remove exceptions. After that, measurements are segmented to remove outliers from unexpected motions. Finally, magnitude peaks in frequency domains are used to detect the heart and respiration rates.

A. System Model

In our solution, an MIMO radar emits a signal $x_k(t)$ at the k-th pulse repetition interval (PRI). When a human is within the detection coverage, the body parts including the heart and chest can be modeled as a collection of reflective points, as shown in Figure 1. As a result, the reflection signal signature $y_k(t)$ at a receiver antenna is a superposition of those reflection signals modulated by each body part independently:

$$y_k(t) = \sum_{0}^{N-1} \rho_i(t) r_i(t) x_k(t) \tag{1}$$
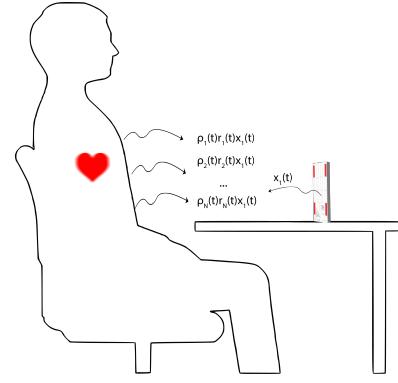

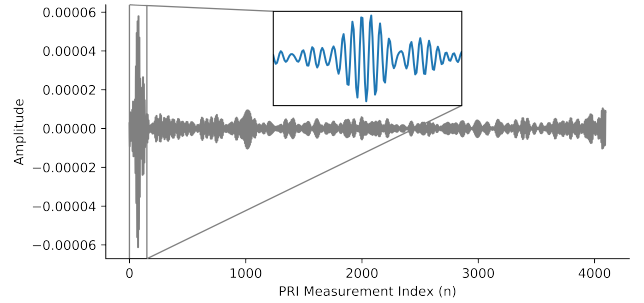Fig. 1. The System model.

Fig. 2. The amplitudes of reflected signals over a PRI.

where N refers to the number of body reflective points including the heart and chest, $\rho_i(t)$ is the complex reflectivity parameter of the body reflective point i, and $r_i(t)$ presents the corresponding round-trip channel response between the radar sensor and the body reflective point i.

It should be noted that the received signal $y(t)$ contains not only reflections from body parts but also those from environment background. We define background reflections as "noise" $n(t)$ to the activity signals. Then $y(t)$ follows:

$$y_k(t) = \sum_{0}^{N-1} \rho_i(t) r_i(t) x_k(t) + n(t) \tag{2}$$

Clearly, $y_k(t)$ contains the signals reflected by the heart and chest. Consequently, the variation of $y_k(t)$ over a number of PRIs also contains the reflection variations due to the heartbeats and respiration.

B. Data Measurements

In our system, a unique novelty is to use a high-frequency data measurement at kHz to capture the highly fine dynamics of a reflection signal due to any motions in each PRI. Specifically, $y_k(t)$ is measured of 4096 times equally over a PRI, which captures the reflections from the objects at a fine spatial resolution of $\frac{1}{4096}$. An example is shown in Figure 2, which has 35 for the pulse repetition frequency (the inverse of PRI).

To capture the signal reflection variations due to heartbeats and respiration, we reformat the measurements according to the measurement indices in a PRI. Therefore, the k-th PRI
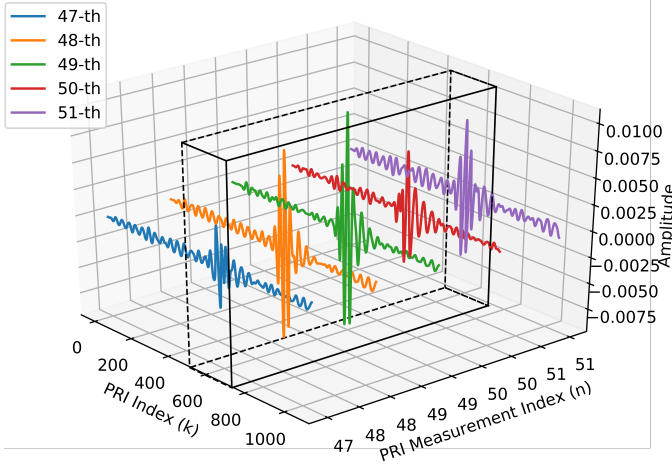
Fig. 3. Rearranged measurements over 1000 RPIs according to the measurement indices within a PRI. There only shows 5 out of 4096 measurements for illustration.

results in 4096 measurements $y_k(n)$ where n refers to the n-th measurement with $n \in [0, 4095]$. Then, $y_k(n)$ with $k \in [0, K]$ are the measurements at the index n over K PRIs, which contains the spatial variations of a reflective point contributing to the measurements at the index n. An example is plotted in Figure 3 where each sequence represents the amplitudes measured at a particular index over 1,000 PRIs, with the reflected noisy motions, which have higher amplitudes than that of the surrounding periodical parts, highlighted with the boxed area.

C. Motion Localization

Within each PRI, although the very high-resolution measurements at 4096 Hz can capture a wide range of motions in the surrounding, it is obvious that the heartbeats and the respiration will only result in impacts on a certain range of measurement indices, not all of them, which can be clearly observed from Figure 2, for example, where the motions are captured by measurements $y_{k_0}(n)$ with $n \leqslant 200$ on the left portion of the diagram. As a result, the measurement temporal sequences at other indices will mostly contain no motions. Elimination of these measurements without motions will definitely improve the computation efficiency and the detection accuracy because only a few sequences are retained and the motion signals are less interfered by other sequences.

We design a standard deviation based motion signal selection scheme. Intuitively, the measurement sequences with motions will fluctuate in amplitudes, which results in large standard deviations. Those measurements with standard deviations less than a threshold are excluded for further processing.

D. Data Preprocessing

Before we perform detections of heart and respiration rates, the static background and the motions other than the heartbeats and respiration in the background should be removed.

1) Background Removal: To remove the static background reflections, the system first keeps sensing the environment and obtains the average static background reflections from a number of PRIs: $\bar{y}_k$.

Then, background removal in the detection stage is implemented as the measurements at each PRI index subtract its background reflection average: $y_k - \bar{y}_k$.

2) Frequency Filtering: Sometimes, abrupt and unexpected interferences result in overwhelmingly large reflection amplitudes that completely overshadow the reflections due to heartbeats and respiration. To address this problem, after the static background reflections are eliminated, a Butterworth bandpass filter is employed to remove those frequency components that are beyond the range of heartbeats and respiration. The Discrete Fast Fourier Transformation (DFFT) magnitudes for the sequence of temporal measurements at the n-th index can be defined as:

$$F^{'}(\omega, n) = \sum_{p=0}^{K} X(p, n)\delta(p\frac{2\pi}{N} - \omega) \qquad (3)$$

where ω is the frequency, K is the length of the measurement sequence of $y_k(n)$. The $X(p, n)$ is the p-th FFT magnitude. $p\frac{2\pi}{N}$ converts the magnitude index p to the frequency ω. Then the frequency components remained after the Butterworth filtering are:

$$F(\omega, n) = |F^{'}(\omega, n)| \cdot |H(\omega - (\omega_l + \omega_c))^2| \qquad (4)$$

where the H is the function of Butterworth filter, and ω_l, ω_c respectively denote the low-cut and high-cut frequencies of the bandpass filter.

E. Elimination of Non-periodic Signals

Another challenge is to work on the reflection signals with motions other than heartbeats or respiration. For example, the motions of arms, body, or fingers will result in interference to the reflections. One observation is that these unexpected motions are very likely non-periodic. In time domains, the abrupt energy of reflections from these motions could mask out that of heartbeats or respiration motions if these motions overlap.

To address this non-periodic interference issue, we design a sliding window plus a segmentation scheme. First, a sliding window is applied to a temporal measurement sequence $y_k(n)$. Then each window of measurements is partitioned into two equal-sized segments. The sliding window makes as many measurements as possible to reserve the periodicity of heartbeats and respiration, while the segmentation is used to locate and isolate the non-periodic components. An example is shown in Figure 4 of this process. At the top, a sliding window with size 340 is applied and then each window is divided into two segments of 170 measurements each.

After the segmentation, with the observation that non-periodic temporal signals are transformed into small background frequency components on the FFT spectrum, our system performs the FFT on each segment. Then, a ratio
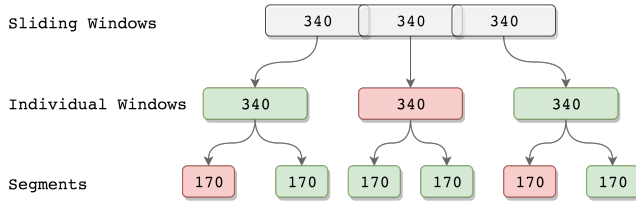
Fig. 4. Sliding window with segmentation partitions the temporal measurements to isolate interferences and non-periodic unwanted motions.
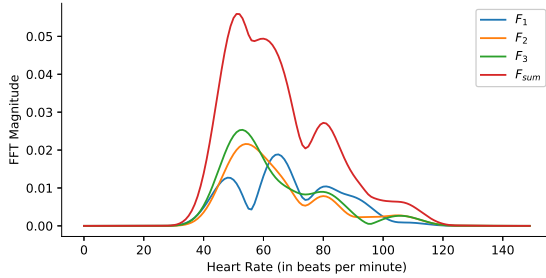

Fig. 5. Superposing FFT magnitudes to reduce the impact of the defective measurements of F_1 on the detection.

measuring the periodicity is computed for each segment, which is defined as the dominant FFT magnitude divided by the average FFT magnitude. A segment is excluded from the data pool if its periodicity ratio is smaller than a preset threshold.

F. Rates Detection

After data has been preprocessed with background, interferences and unconcerned frequency components removed, the rates detection is performed as below.

1) Superposing FFT magnitudes: With tens of PRIs in each second and each PRI is sampled at 4096Hz, it is obvious that the periodic heartbeats and respiration will result in periodic variations of the amplitude measurement $y_k(n)$ at each sample index. To avoid any sample exception or deficiency, we superpose the FFT magnitudes of the concurrent measurement sequences at the indices retained after the preprocessing. The superposition can make the peak magnitudes prominent, which are corresponded to the heart/respiration rates. For example, as Figure 5 shows, the three curves stand for the FFT magnitudes corresponding to heart rates that are converted from frequencies. Superposing three curves relieves the impact of the error peak of the curve F_1, and the heart rate corresponding to the peak magnitude of the superposed curve is taken. The superposition operation is performed as:

$$F_{sum} = \sum_{j \in A} \sum_{n \in C} F_j(\omega, n) \qquad (5)$$

where the set C is a collection of indices of retrained measurement sequences after the date preprocessing as described in Section III-D, and the j denotes the identity of antenna pairs in the collection of antenna pairs A.

The superposition of FFT magnitudes is also performed to the measurements from different antenna pairs. Denoting the measurements from two antenna pairs as $S_k(n)$ and $H_k(n)$, the new sets of measurements, concurrently captured from the same implementation would be: $M = \{S_k(1), S_k(2), ..., S_k(n), H_k(1), H_k(2), ..., H_k(n)\}$. Refer to Section III-B for more details of the equation. Using multiple sources of time-series signals provides more references for correcting errors, and produces a commonly acknowledged result by multiple concurrent temporal measurement sequences.

2) Rates Determination: After the superposition is performed to each window of measurements, which is the divided temporal measurements as Figure 4 shows, the frequency that has the peak magnitude in the F_{sum} is considered as the heart rate.

IV. PERFORMANCE EVALUATION

We have implemented the solution on a testbed and evaluated the performance with a medical device.

A. Ground Truth

An FDA-approved Bluetooth fingertip pulse oximeter is used for the ground truth of heart rates. The oximeter measures heart rates by sensing the light abortion degree from shining the light into the skin [17]. The heart rate data are logged onto a mobile phone via Bluetooth. The oximeter generates a heart rate based on the continuous measuring for every 30 seconds, using its built-in algorithm.

B. Experiment Settings

An FMCW radio-frequency-based radar sensor, called Walabot, is used, and its bandwidth ranges from 3.3 to 10.3 GHz. The maximum spatial resolution is about 2 cm. Four antennas are used in capturing reflected signals from different angles and directions, though the device supports up to 18 antennas [18]. The device's PRF (Pulse Repetition Rate) is 35 Hz. Based on the Nyquist sampling theorem, the maximum detectable frequency is 17.5 Hz, which is equivalently 1050 heartbeats per minute. Namely, the PRF is far more than enough to detect regular heartbeats. The average transmit power is about -16 dBm, so it can only support detection within a short range in the experiments. For the software, our solution is implemented in Windows 10 with the data measurements from the Walabot API (Application Programming Interface).

The experiments have been performed in a regular lab office. As Figure 1 presents, the sensing device is placed on the table, with the antennas on the front pane facing the subject's chest, who sits at the table. The subject also wears the finger pulse oximeter connected to a smartphone for logging ground truth data. The distance between subject's chest and the radar sensor is limited to 1 m to achieve the best measuring outcome.

C. Performance on Accuracy

We have evaluated the accuracy of detecting respiration and heart rates in various situations.
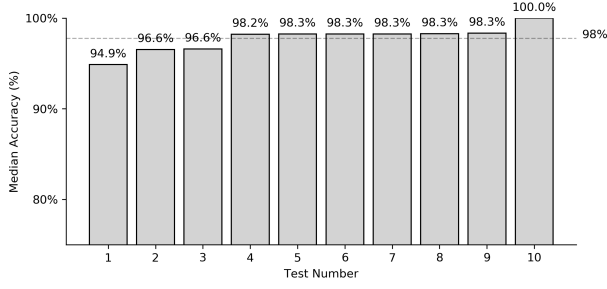
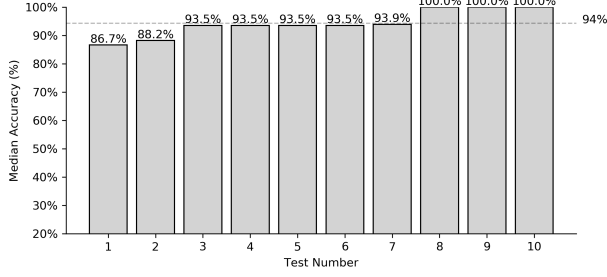Fig. 6. The accuracies as the subject keeps still.

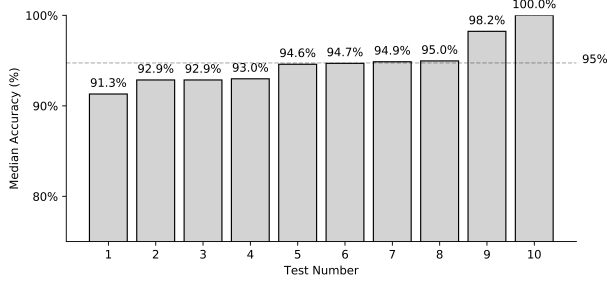Fig. 7. The respiration rate accuracies with the static subject

Fig. 8. The accuracies as the subject fingers operating a mobile phone.

1) Rates Detection with Quasi-Static Subjects: The first test is on the detection accuracy when the subject is quasi-static without any other body parts moving. We test the detection of both heart rates and respiration rates. There are 10 independent experiments conducted. For each experiment, the radar sensor keeps recording the data for 30 seconds.

The first case is for the heart rate. To capture the heart rate changes in each second, the sliding windows size is set to 35 measurements corresponding to the average sampling frequency of 35 Hz. The radar sensor is placed 0.5 m away from the subjects, placed on the table as Figure 1 shows.

The performance is plotted in Figure 6. The accuracy is computed as the percentages to the ground truth. The experiment results are arranged in the ascending order on the figure. The average accuracy is above 98%, which is represented by a horizontal dotted line.

The respiration rate result is shown in Figure 7. The average respiration rate is 94%. Most of the detection give the accuracy over 93.5%.
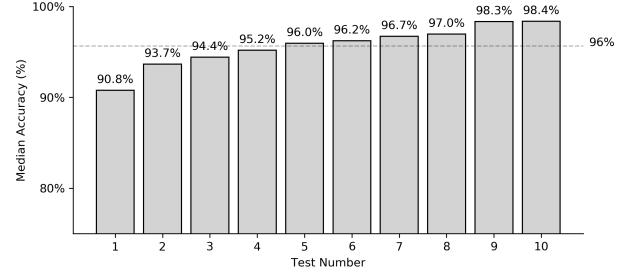

Fig. 9. The accuracies as the subject slightly moves body back and forth.

2) Body and Finger Movements: This test is to measure the accuracy when the noises of finger motions are involved. The test setup is as in the above test. A mobile phone is placed on the table between the subject and the radar sensor. In the test of 30 seconds, the subject randomly operates the mobile phone as in daily use for totally 2 seconds, e.g., sliding on the screen or clicking on the button. The test is repeated 10 times.

The results are plotted in Figure 8 as arranged in the ascending order of the accuracy. As we can observe, the finger motions do incur some interferences to the detection accuracy, but the overall performance is still high, with an average of 95%.

In addition, we have also tested the accuracy when the whole body is in motion. In this case, the subject swings the body back and forth slightly every 10 seconds and 10 experiments are implemented. Those actions would result in a series of non-periodic signals to the measurement. Figure 9 shows the average accuracy for the body movements of 96%.

3) Antenna Pairs: It is of utmost interest to see the accuracy performance for a different number of antenna pairs. All the antennas are evenly distributed on the front board. The layout of the four antennas is arranged as a square with antennas fixed at the four corners [18]. Totally three combinations of transmitting and receiving antennas are used. Four antennas are numbered as 1, 17, 4 and 18. Three antenna pairs chosen from the combinations are 1→17, 17→4, and 4→18.

Three pairs of antennas capture the reflections simultaneously for 30 seconds in each experiment, and totally 10 experiments are performed. To show the advantages in dealing with noises, the tests are performed with the noises of finger movements for totally 2 seconds in each test.

In order to eliminate the influence of the antenna layouts and for fairness, three accuracies from three individual antenna pairs are averaged to get the final average accuracy for the one pair of the antenna case. Similarly, the average performance is evaluated for the two pairs of antennas, and there is only one accuracy for utilizing all three antenna pairs simultaneously.

The performance data for the combinations of antenna pairs are presented in Table I. As the data shows, the accuracy is higher when using more than one antenna pair. In the case of one pair, the worst accuracy among the antenna pairs is only 91.7% with the average accuracy of all pairs as 94.4%. As more antenna pairs are exploited, the average performance

	Combination				
Number	1→17	17→4	4→18	All	Average
1	98.6%	92.9%	91.7%	∅	94.4%

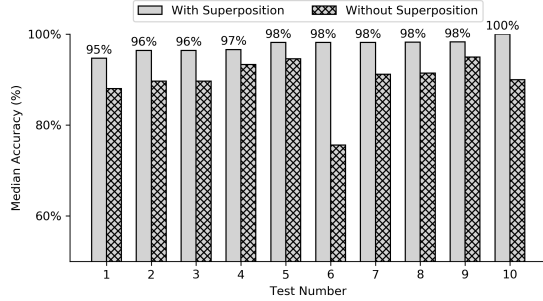|	Combination				
Number	1→17&17→4	17→4&4→18	1→17&4→18	All	Average
2	98.4%	98.0%	94.4%	∅	96.9%
3	∅	∅	∅	98.2%	98.2%

Fig. 10. The accuracies with and without the superposition. The sets without superposition simply take the average heart rates detected on different sequences.

is improved. When all three pairs are used, the accuracy is increased to 98.2%. It indicates the MIMO approach to the detection has various advantages.

4) Correction with Superposition: This experiment is designed to verify the effectiveness in addressing exceptions by superposing FFT magnitudes of the measurements at various indices from multiple antenna pairs as in Section III-F1 and Figure 4. The experiment uses three pairs of antennas, and each pair contributes five measurement sequences (at five indices) with 15 heart rates generated in each window. Its performance is compared with the case without the superposition correction that only takes the average values of 15 heart rates.

The results are shown in Figure 10. Overall accuracy with superposition overpasses that without it, where the average accuracy with superposition is 98% while that of those without superposition is about 90%. Especially in the 6-th bin, the accuracy is improved by 20%. A conclusion can be drawn that the superposition can mostly improve the accuracy of detection.

V. CONCLUSION

In this paper, we propose a solution to the non-contact non-invasive heart and respiration rates monitoring, by using an MIMO FMCW radar, capturing the amplitudes of the reflections from subjects. With very high resolution of measurements (4 KHz) in each PRI, heart and respiration rates can be extracted from the compound motions of the heart and chest. The use of multiple antennas complements detection defects and unexpected interferences. Furthermore, the superposition of multiple detection indices within each PRI improves the accuracy more. With extensive experiments in the real world, the proposed system shows strong reliability and high accuracy in detecting both heart and respiration rates simultaneously.

REFERENCES

[1] X. Yang, G. Sun, and K. Ishibashi, "Non-contact acquisition of respiration and heart rates using doppler radar with time domain peak-detection algorithm," in *2017 39th Annual International Conference of the IEEE Engineering in Medicine and Biology Society (EMBC)*, July 2017, pp. 2847–2850.

[2] L. Ren, H. Wang, K. Naishadham, O. Kilic, and A. E. Fathy, "Phase-based methods for heart rate detection using uwb impulse doppler radar," *IEEE Transactions on Microwave Theory and Techniques*, vol. 64, no. 10, pp. 3319–3331, Oct 2016.

[3] W. Wei and P. Yingning, "An interpolation algorithm to improve range estimation for the linear frequency modulated radar," *IEEE Aerospace and Electronic Systems Magazine*, vol. 14, no. 7, pp. 45–47, Jul 1999.

[4] M. Sekine and K. Maeno, "Non-contact heart rate detection using periodic variation in doppler frequency," in *2011 IEEE Sensors Applications Symposium*, Feb 2011, pp. 318–322.

[5] I. V. Mikhelson, S. Bakhtiari, T. W. E. II, and A. V. Sahakian, "Remote sensing of heart rate and patterns of respiration on a stationary subject using 94-ghz millimeter-wave interferometry," *IEEE Transactions on Biomedical Engineering*, vol. 58, no. 6, pp. 1671–1677, June 2011.

[6] R. Steele, A. Lo, C. Secombe, and Y. K. Wong, "Elderly persons perception and acceptance of using wireless sensor networks to assist healthcare," *International Journal of Medical Informatics*, vol. 78, no. 12, pp. 788 – 801, 2009, mining of Clinical and Biomedical Text and Data Special Issue. [Online]. Available: http://www.sciencedirect.com/science/article/pii/S1386505609001178

[7] H. Wang, D. Zhang, J. Ma, Y. Wang, Y. Wang, D. Wu, T. Gu, and B. Xie, "Human respiration detection with commodity wifi devices: Do user location and body orientation matter?" in *Proceedings of the 2016 ACM International Joint Conference on Pervasive and Ubiquitous Computing*, ser. UbiComp '16. New York, NY, USA: ACM, 2016, pp. 25–36. [Online]. Available: http://doi.acm.org/10.1145/2971648.2971744

[8] W. Hu, H. Zhang, Z. Zhao, Y. Wang, and X. Wang, "Real-time remote vital sign detection using a portable doppler sensor system," in *2014 IEEE Sensors Applications Symposium (SAS)*, Feb 2014, pp. 89–93.

[9] R. El-Bardan, D. Malaviya, and A. D. Rienzo, "On the estimation of respiration and heart rates via an ir-uwb radar: An algorithmic perspective," in *2017 IEEE International Conference on Microwaves, Antennas, Communications and Electronic Systems (COMCAS)*, Nov 2017, pp. 1–5.

[10] M. Bradley, "Frequency-modulated continuous-wave (fmcw) radar," http://demonstrations.wolfram.com, from the Wolfram Demonstrations Project.

[11] F. Zhao, M. Li, Y. Qian, and J. Z. Tsien, "Remote measurements of heart and respiration rates for telemedicine," *PLOS ONE*, vol. 8, no. 10, pp. 1–14, 10 2013. [Online]. Available: https://doi.org/10.1371/journal.pone.0071384

[12] C. Takano and Y. Ohta, "Heart rate measurement based on a time-lapse image," *Medical Engineering & Physics*, vol. 29, no. 8, pp. 853 – 857, 2007. [Online]. Available: http://www.sciencedirect.com/science/article/pii/S1350453306001901

[13] G. Balakrishnan, F. Durand, and J. Guttag, "Detecting pulse from head motions in video," in *2013 IEEE Conference on Computer Vision and Pattern Recognition*, June 2013, pp. 3430–3437.

[14] T. Sirkis, Y. Beiderman, S. Agdarov, Y. Beiderman, and Z. Zalevsky, "Monitoring blood vital bio signs using secondary speckle patterns," *Opt. Express*, vol. 24, no. 24, pp. 27 899–27 909, Nov 2016. [Online]. Available: http://www.opticsexpress.org/abstract.cfm?URI=oe-24-24-27899

[15] Y. Beiderman, I. Horovitz, N. Burshtein, M. Teicher, J. Garcia, V. Mic, and Z. Zalevsk, "Remote estimation of blood pulse pressure via temporal tracking of reflected secondary speckles pattern," *Journal of Biomedical Optics*, vol. 15, pp. 15 – 15 – 7, 2010. [Online]. Available: https://doi.org/10.1117/1.3505008

[16] Y. Sun and N. Thakor, "Photoplethysmography revisited: From contact to noncontact, from point to imaging," *IEEE Transactions on Biomedical Engineering*, vol. 63, no. 3, pp. 463–477, March 2016.

[17] P. Mohapatra, S. P. Preejith, and M. Sivaprakasam, "A novel sensor for wrist based optical heart rate monitor," in *2017 IEEE International Instrumentation and Measurement Technology Conference (I2MTC)*, May 2017, pp. 1–6.

[18] *Walabot-Technical Brief*, https://walabot.com/docs/walabot-tech-brief-416.pdf, Walabot.